Nano Express

ACCEPTED MANUSCRIPT • OPEN ACCESS

Au – MoS_2 nanoflowers sensors on interdigitated electrode for monitoring human respiration

To cite this article before publication: Sakshi Pujari *et al* 2024 *Nano Ex.* in press https://doi.org/10.1088/2632-959X/ad6c67

Au – MoS_2 nanoflowers sensors on interdigitated electrode for monitoring human respiration

Sakshi Pujari[1¥], Himadri Tripathi[1¥], Anshuman Dobhal[1], Saurabh Rawat[1], Shivani Dangwal[1], Shashi Bala[2], Chanchal Rani[3], Charu Dwivedi[4], Rajesh Kumar[3], Mohit Sharma[5], Himani Sharma[1*]

[1]Functional nanomaterials Research Laboratory, Department of Physics, Doon University Uttarakhand-248001, India

[2]Government Arya Degree College Nurpur-176202, Kangra, Himanchal Pradesh, India

[3]Materials and Device Laboratory, Department of Physics, Indian Institute of Technology, Indore-453552, India

[4]Department of Chemistry, Doon University Uttarakhand-248001, India

[5]Institute of Materials Research and Engineering, A*STAR (Agency for Science, Technology and Research), 2 Fusionopolis Way, Innovis, #08-03, Singapore 138634, Singapore

Corresponding Author: Himani Sharma

Email ID: himanitiet427@gmail.com

Abstract

Respiratory sensors are emerging as powerful tools for continuous, non-invasive monitoring of breathing patterns. These sensors hold immense potential for applications in various healthcare scenarios. In this paper, we report a novel transition metal dichalcogenides (TMDC's) based respiratory sensor that exhibits high resistivity, fast response, and excellent flexibility. TMDC turned out to be the most suited of all materials as they offer tunable bandgap with wider surface area resulting in higher sensitivity to specific targets. MoS_2 (Molybdenum Disulfide), a TMDC, has emerged as a promising material for developing next-generation respiratory sensing devices while its hybrids with Au nanoparticles enhances the electrical conductivity of the sensor, providing better performance than either material alone. This paper explores the potential advantages of Au-MoS_2 based sensors for respiratory monitoring applications.

In context to that, present work focuses on the resistivity and flexibility of hybrids for respiratory sensing. The MoS_2 nanoflowers are synthesized by hydrothermal method further using inert gas deposition method for the decoration of Au nanoparticles over MoS_2. To form Au-MoS_2 hybrids, Au nanoparticles were decorated over MoS_2 using inert gas deposition. The crystallinity of the hybrids is studied using Raman Spectroscopy and X-Ray Diffraction techniques. The morphology of the samples was studied through scanning electron transmission (SEM) while Au nanoparticles were detected on the edges of MoS_2 by transmission electron microscope (TEM). The interfacial electronic interaction and binding energies were detected using X–Ray photoelectron spectroscopy (XPS) and ultraviolet photoelectron spectroscopy (UPS). The study tested a respiratory sensor in a simulated environment, finding it more responsive to breathing and quick to return to rest. This suggests potential for the Au-MoS_2 sensor in tracking breath states due to its sensitivity and adaptability, promising applications across various fields.

Introduction

One of the most important aspects of evaluating health is breath monitoring. Conventional approaches are less efficient in particular situations because they frequently depend on visual observation or substantial equipment[2]. Respiratory sensors are useful in this situation. These non-invasive tools are intended to observe, record, and evaluate breathing patterns.

Respiratory sensors are instruments that can be used to monitor a variety of respiratory parameters, including respiratory rate, respiratory volume, and exhaled gas composition[3,4]. These variables can be used to diagnose respiratory disorders and evaluate the condition of the respiratory system. They are made to detect, measure, and interpret respiratory data in real-time outfitted with cutting-edge technology [5].

Respiratory sensors can incorporate in fitness and wellness tracking. Additionally, it can aid in the early detection of chronic diseases, post-operative care, and the identification of possible sleep apnea or other breathing variations. With the rapid advancement of technology, breathing sensors may soon find use in the monitoring of mental health[6].

Recently Transition metal dichalcogenides (TMDCs) based respiratory sensors have attracted great attention. TMDCs have a tunable bandgap, which allows for the adjustment of their light absorption and emission properties, enabling the development of sensors that respond to certain light wavelengths, in contrast to graphene, which has a zero bandgap that makes it challenging to target specific molecules that are necessary for sensing[7]. The target analyte, or the substance being detected, might interact with the sensor material more readily due to its larger surface area, which could result in a higher sensitivity when detecting the target's existence and quantity[8]. When it comes to sensors that need to be highly sensitive to certain target molecules, TMDCs present a strong solution[9].

Molybdenum disulfide (MoS_2) is the most promising of all the TMDCs because of its multilayered structure and special electrical and optical qualities, which have a potential future in sensing[10]. The layered structure of MoS_2 is like that of graphite and consists of sandwich units with three atom layers (S-Mo-S) piled through Vander Waals forces and possess exceptional electrical properties which has multiple possible usage for gas adsorption. The detection of some gases by intrinsic MoS_2 is still limited after several applications. In the field of gas sensing, its low selectivity makes it easily triggered by other gases, such as water vapour or carbon dioxide[11]. Also, it is difficult to fabricate large area sensors which makes resist its application in commercial purposes. However, its doping with other elements like Au, Cu, Pd have been successful in enhancing the gas sensing performance[12]. Yan et al. (2016) provided evidence of the effectiveness of enhancing the surface of metal oxide-based gas sensors with noble metals (Au) to increase their gas detecting capability. They reported that Au particles assist the detection of ammonia at low temperature because the presence of Au increased the material's capabilities as a novel gas sensing material. Furthermore, Zhou et al. [13] in their research how a layered MoS_2 nanosheet with an Au nanoparticle could detect a NO_2 gas in a recoverable, sensitive, and selective manner at ambient temperature. He claimed that the added Au particles boosted both the number of active adsorption sites and the diffusion rate in addition to speeding up the transfer of adsorbed species from active to inactive sites. This opens the door to a unique approach for room-temperature Au-MoS_2 based hybrids to be used in the construction of high-performance respiratory sensors[14].

In this work, we fabricated a mask that combines the benefits of gold and is built as a respiratory sensor on MoS_2.[11] The sensor is a resistive type which measures the human breath. The sensor showed enhanced breathing patterns with a high rate of recovery when combined with gold particles[15]. It is determined to be a portable system for monitoring human respiration because of its quick response time and sensitivity[13,16–18].

Materials and Methods

Synthesis of MoS_2 Nanoflowers based sensor:

MoS_2 nanoflowers were synthesized using hydrothermal synthesis.[19] The standard precursor concentration was determined to be 5 gm of thiourea (Sisco Research Laboratory) and 0.8 gm of ammonium molybdate (Sigma Aldrich 99.9% pure), were made transparent by diluting them in 50 millilitres of deionized water (DI) and stirring them for 30 minutes with a magnetic stirrer.

After that, the solution was autoclaved for eighteen hours at 200 °C in a 50-cc stainless steel autoclave lined with Teflon [19]. Furthermore, solution was filtered to produce the black precipitates, which were then five times, separately, cleaned with ethanol and distilled water. The MoS_2 nanoflowers was then formed by drying the resulting black precipitate at 70 °C in a hot air oven [[20].

Synthesis of Au-MoS_2 hybrids-based sensor:

Au nanoparticles were decorated via Inert gas deposition to form Au-MoS_2 hybrids. Prior to being placed inside the growing chamber, the substrate (glass slides) and Printed Circuit Board (PCB) copper electrodes were fully washed with DI water. For gas sensing performance, PCB copper electrodes were utilised, and tiny glass slides with a standard dimension of 10 mm×10 mm were employed as the characterisation substrate as well. By resistive heating, 99% pure Au foil was evaporated using a molybdenum boat [[19]. The deposition was carried out at a base pressure of 4×10^{-6} Torr by providing 80 A to the boat [[21]. A digital thickness monitor (DTM) was used to measure the thickness of Au films. To prevent Au nanoparticles aggregation, these deposited samples were subsequently annealed at 150°C to 200°C in an Argon gas environment. The size of the nanoparticles is influenced by the difference in vapor pressure between the Au melting surface and the film (which is being deposited) during a metallic film deposition process. Au-MoS_2 was then drop casted on the copper electrodes with thicknesses of 2 nm separately, at deposition pressures of 4×10^{-6} Torr. During inert gas evaporation, the higher areal density of nanoparticles at lower pressure is linked to the higher atom concentration, which encourages accelerated nucleation and tends to create bigger nanoparticles. At lower pressures, compared to higher pressures, the mean free path results in fewer collisions between Au atoms and gas molecules, producing smaller nanoparticles. As a result, larger, denser Au nanoparticles would form on the MoS_2 nanoflowers as more Au atoms would reach the substrate's surface [[19].

Results and Discussions

The crystalline structure of MoS_2 and Au-MoS_2 nanoflowers were confirmed by x-ray diffraction (XRD). The diffraction pattern of bare MoS_2 nanoflowers and Au-MoS_2 nanoflowers can be observed in the figure 1. With an XRD pattern indexed at 13.11∘, 26.44∘,32.26∘, 35.53∘, and 57.07∘, corresponding to the (002), (004), (100), (103), and (110) crystal planes of the MoS_2 structure, both samples demonstrate the crystallite nature of MoS_2 materials[22]. These results are consistent with the relevant standard card (JCPDS card number 371492). Additional minor peaks at 37.7° exist in the case of Au-MoS_2 hybrids, and they correlate to the Au (111) plane (JCPDS card number 040784)[23].

The strength of the peak at the (002) and (004) planes was lowered by the addition of gold nanoparticles. This is because there are less well-defined layers that contribute to the signal when gold particles are added, disrupting the ordered stacking of MoS_2 layers and lowering intensity. Because the addition of Au altered the material's crystallinity, frequently indicating smaller crystallite sizes or a wider spread of crystallite sizes, the peak likewise became more widely distributed at (004), (100), (103) planes [22].

Micro-Raman spectroscopy (μRS) was used to analyze the atomic vibrational modes of the bare and Au decorated MoS_2 hybrids [19]. The excitation wavelength used for Raman spectroscopy is 533 nm. Figure 2 represents μRS of bare MoS_2 and Au-MoS_2 hybrids. The peaks were observed at 377 cm^{-1} and 405.4 cm^{-1} [24]. The gap of 28.4 cm^{-1} indicates that 2D flakes of the nano petals of MoS_2 are present in bulk. In addition to the frequency change, the Au-MoS_2 hybrids show a rise in peak intensity with increasing Au NPs size. The addition of Au nanoparticles slightly shifted the peak at 383 cm^{-1} and 408 cm^{-1} inferring an increase in the layers of MoS_2 from the sample [[25]. Because a locally amplified electric field is created on the surface of the Au nanoparticles, the Raman intensity increases dramatically when the plasmon oscillation frequency is in resonance with the photon frequency of the input light. There are side peaks for both E and A mode in Au -MoS_2 sample (Figure 2). The introduction of gold nanoparticles was the source of the side origin of side peaks at the A_{1g} and E^1_{2g} modes [24]. The coupling of strain and lattice vibrations, as well as the interactions of various phonon modes within the Au -MoS_2 compound, caused by the addition of Au, resulted in new peaks and altered surface morphology [22]. The Raman spectra of MoS_2 nanoflowers exhibit a third peak at 452 cm^{-1}, which can be attributed to the second-order longitudinal acoustic phonon (2LA(M) mode) at the M point [26]. Remarkably, both modes' intensities increased as the reaction time increased, indicating that MoS_2 nanoflowers' crystallinity had improved. First-layer effect arising from the emergence of extra Raman modes around 379 cm^{-1} and 397 cm^{-1} (the latter is called the A_{1g} reduced mode in the following) is specific to MoS_2 in direct contact with the Au surface. The normal Raman modes get more intense as the number of layers increases, while the extra modes nearly always stay at the same position and intensity [22]. The mode around 379 cm^{-1} can be interpreted as the E^1_{2g} mode of strained MoS_2.

The morphology of MoS_2 was imaged using FESEM which confirmed the flower like structure [26]. The findings showed that no additional nanoparticles were confirmed and that their existence had no impact on the characteristics of MoS_2 nanoflowers [22]. Figure 3(a) and 3(b) depicts the same. Furthermore, TEM imaging [23] of bare MoS_2 and Au-MoS_2 hybrids was performed as shown in figure 3(c) and 3(d) respectively. The HRTEM images attest to the presence of Au nanoparticles and a structure like a flower. Au nanoflowers typically have a more uniform and spherical morphology compared to MoS_2 nanoflowers, which have a more irregular and plate-like structure. Thus, as per SEM images and TEM analysis Au nanoparticles are uniformly distributed across the surface of MoS_2.

XPS characterisation was used to further investigate the electrical interaction at the interface between the Au-MoS_2 hybrid and the bare MoS_2 and Au-MoS_2 hybrids, as well as the elemental composition and chemical states of both samples (Figure 4). The obtained samples contain Mo, S and Au, which are verified by the examination of the XPS patterns. The Mo_{3d} XPS scan is displayed in Figure 4(a) where two major peaks are observed at 228.3 and 232.5 eV, respectively, and are attributed to $Mo3d_{5/2}$ and Mo $3d_{3/2}$, the presence of the Mo_{4+} oxidation state.

The lower side change in the binding energy is caused by the electrical interaction between Au and MoS_2 at the interface. The increased work function of Au could be an indication of the formation of a Schottky barrier at the contact that transfers electrons from MoS_2 to Au. As a result of this contact, the interface is modified, which increases electron availability since Au particles have a higher electronegativity and hence decreases hybrid resistivity and improves the capacity to sense gases.

Figure 4(b) displays the Au XPS spectra for MoS_2 and Au-MoS_2 hybrids. The in situ generated Au particles have been identified as the source of two unique peaks, Au $4f_{7/2}$ and Au $4f_{5/2}$, respectively, at 84 eV and 87.7 eV. Figure 4(c) shows XPS spectra of S 2p. The S peak breaks into two peaks at 162.8 eV and 161.6 eV, which correspond to the S $2p_{3/2}$ and S $2p_{1/2}$ orbitals of S 2p, respectively[19]. These peaks are observed to be slightly wider and lower shift when Au particles are decorated on the surface, indicating surface modification. The S 2p nanoparticles were stabilized by the presence of Au, which also changed the electron charge density surrounding the S atom and the binding energy and peak shape of the XPS spectrum. Figure 4(d) displays the XPS spectra of the O 1s. Its peak was observed at 531 eV and 532.4 eV [19,27].

Figure 5 represents the valence band edge and secondary electron cutoff for MoS_2 and Au-MoS_2 acquired from the UPS. As shown in figures 4(a)-(b), the valence band maxima for MoS_2

(MS) and Au- MoS_2 (Au-MS) were 3.68 and 3.655 eV, respectively, which is 0.025 less than that of MoS_2. This discrepancy suggests that the Au-MoS_2 material is slightly more reactive and sensitive than MoS_2 alone because it has a little inclination to receive electrons. The work function obtained for bare MoS_2 and Au-MoS_2 hybrids were found to be 4.45eV and 4.23eV respectively, which tells us that the work function is decreased by 0.22eV when the sensor was decorated with Au on the surface. Moreover, it confirms that the Schottky barrier creation at the interface is causing an electron transfer from MoS_2 to Au nanoparticles. As a result, this interaction improves the gas detecting capability[19,21].

Respiratory Sensors and Mask Design

The hybrid Au-MoS_2 solution was evenly drop casted onto the PCB copper electrode of size 2.2cm ×3.2cm as shown in figure 6(a). The sensor was then mounted on a cotton mask so that the wearer could easily operate it. To protect the copper-plated threads that functioned as electrodes, an electrode cover made of a hydrophobic material was used [[27]. The thyristor (sensor) was mounted in the mask so that it sits between the nose and the mouth and detects breathing. This allowed the sensor to be stabilized at the correct location. Further, human breath was recorded using the source metre (Keithley 2450) as shown in figure 6(b), and graphs were created utilising the data [[8]. A schematic representation of the sensor incorporated into the mask is shown in Figure 6(c).

Respiration Monitoring

The sensors work by detecting variations in electrical resistance when exposed to different breathing patterns. The mechanism involves how the interaction between the oxygen molecules and the Au-MoS_2 changes the electrical resistivity of the sensor [[17]. During inhalation, oxygen molecules present in the air may interact with the surface of the sensor. The interaction between them alters the sensor conductivity [[18]. This change in conductivity is thus measured as a change in resistance. While during exhalation, a decrease in the oxygen level is observed, leading to change in the sensor's conductivity, which is again detected and processed [[28]. The respiratory levels were not measured independently along with a change in the conductivity for the mask measurements because variations in the total charge of respiration levels inside a mask depend on the moisture content of each user's breath and the fit of the mask for each user [4]. This arrives to a speculative conclusion that variations in the breathing within the face mask induced by the user's breathing modify the resistance of the final mask platform as they breathe in and out [[29].

The sensor is capable of precisely detecting the moisture in a breath and recovering quickly enough to detect the next breath. The signal quality was steady even when measuring breaths outside. The lingering moisture in the mask between these breaths provides an explanation for this. The resistance was observed to be continuous and capable of returning to its initial value during each breathing study [[30,31]. Figure 7 displays the response curve that was created by repeatedly measuring the user's breathing patterns in order to assess the sensor's repeatability. The amplitude variations of the various breathing patterns were shown by the graphs in Figure 8. Normal breathing, as depicted in figure 8(b), lies in the amplitude range between shallow breathing in figure 8(a) and deep breathing in figure 8(b) [32]. The increase in the electrode resistance also suggested that the humidity level had increased. As a result, it concluded that Au-MoS_2 solution, rather than MoS_2, was a superior choice for the sensor since it was very sensitive and hence more easily able to capture changes in the breathing pattern [33].

The breathing response curve at various parameters is shown in Figure 9. Talking while walking curve in figure 9(b) exhibits a pattern with considerable consistent fluctuations, while no talking while walking curve in figure 9(a) shows a dramatic decline in resistance in addition to various variations. Furthermore, as shown in figure 9(c), the sensor was able to differentiate between nasal breathing and regular breathing. It shows a smoother curve for nasal breathing as opposed to oral breathing since the slopes obtained were varied based on the amount of moisture expelled [[31].

Additionally, figure 9(d) presents a comparison between coughing and normal breathing, revealing the relative changes observed in the device signals. When we cough, the resistance changes more dramatically, making the slope steeper than it would be when we breathe normally. [34]. A tabular representation of the latest research on respiratory sensors, with an emphasis on the many metrics depicted in figure 10.

Conclusions

To summarise, the analysis of decorated copper electrodes covered with MoS_2 and Au-MoS_2 is done to explore the possible benefits of Au over MoS_2 based sensors concerning respiratory monitoring applications. After being exposed to gold particles, the sensor shows a higher recovery rate, which enhances our breathing patterns[35]. This makes the development of a high-performing respiratory sensor possible. In this work, we constructed a mask that functions as a respiratory sensor on MoS_2 and combines the advantages of gold. X-ray diffraction (XRD) was used to confirm the crystalline structure of MoS_2 and Au-MoS_2 nanoflowers, and the results were consistent with the JCPDS. It was noticed that the ordered stacking of MoS_2 layers at (002) and (004) was disrupted by the addition of Au, decreasing its intensity and similarly widely dispersed peaks at planes (004), (100), and (103). The SEM images confirmed the successful formation of Au-MoS_2 hybrids with distribution of Au nanoparticles on the MoS_2 nanosheets. According to micro-Raman spectroscopy, the vibrational modes were confirmed with the peak positions of 377 cm^{-1} and 405.4 cm^{-1}, indicating a change in frequency and an increase in peak strength. Due to a locally enhanced electric field on the Au surface, the inclusion of Au nanoparticles caused the peak to shift to 383 cm^{-1} and 408 cm^{-1}. Strong interactions with incident light caused by surface plasmon resonance on the gold nanoparticle split the Raman Peak at 452 cm^{-1}. It also demonstrates that as reaction times grew in tandem with mode intensities, the crystallinity of MoS_2 nanoflowers improved. Moreover, the Schottky barrier formation at the interface was verified by UPS and XPS, providing us with evidence that the Au-MoS_2 sample has undergone modifications. The availability of electrons increased as a result of the Schottky barrier formation raising Au's work function[36]. The slightly wider and lower shift in the S peaks, which indicates the surface change, was also caused by the addition of Au. Because the Au-MoS_2 material has a little inclination to receive electrons, the valence band maxima for both MoS_2 and Au-MoS_2 were 0.025 less, suggesting that the Au-MoS_2 material is somewhat more reactive. Similarly, the work function was reduced by 0.22 eV when the sensor's surface was decorated with Au. Au thus improved the sensor's properties to some extent and had a high rate of recovery. Its sensitivity and fast response time lead to the conclusion that it is a portable system for monitoring human breathing. With the speed at which technology is developing, improving breathing sensors can help with post-operative care, early chronic illness detection, and the diagnosis of potential sleep apnea or other breathing abnormalities. Equipped with state-of-the-art technology, it may be made to detect, measure, and interpret respiratory data in real-time.

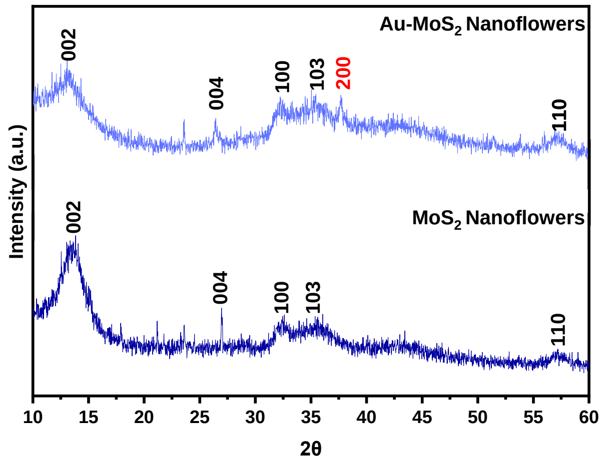

Figure1: XRD pattern of bare MoS_2 and Au-MoS_2 nanoflowers confirming their crystalline pattern.

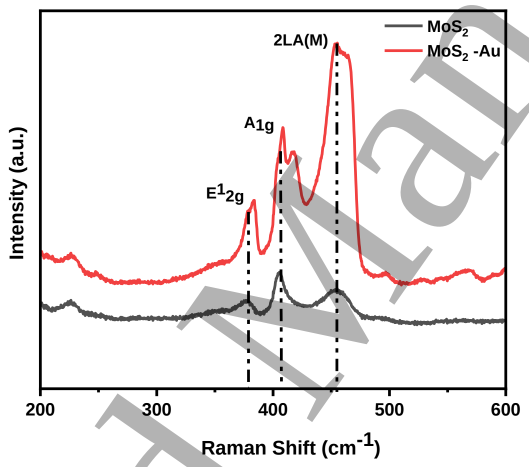

Figure 2: Raman Spectra of bare MoS_2 and Au decorated MoS_2 confirming the formation of MoS_2 in bare MoS_2 and Au-MoS_2 hybrids.

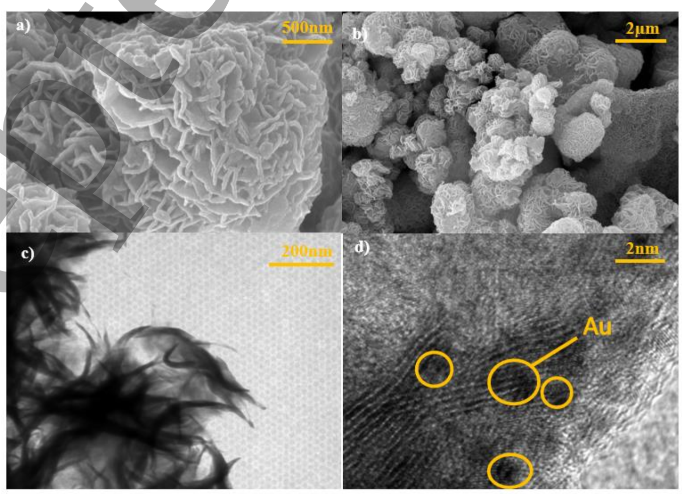

Figure3: FESEM images of (a)-(b) bare MoS_2 nanoflower, HRTEM images of (c) bare MoS_2 (d) Lattice fringes of MoS_2-Au with Au particle size 2nm

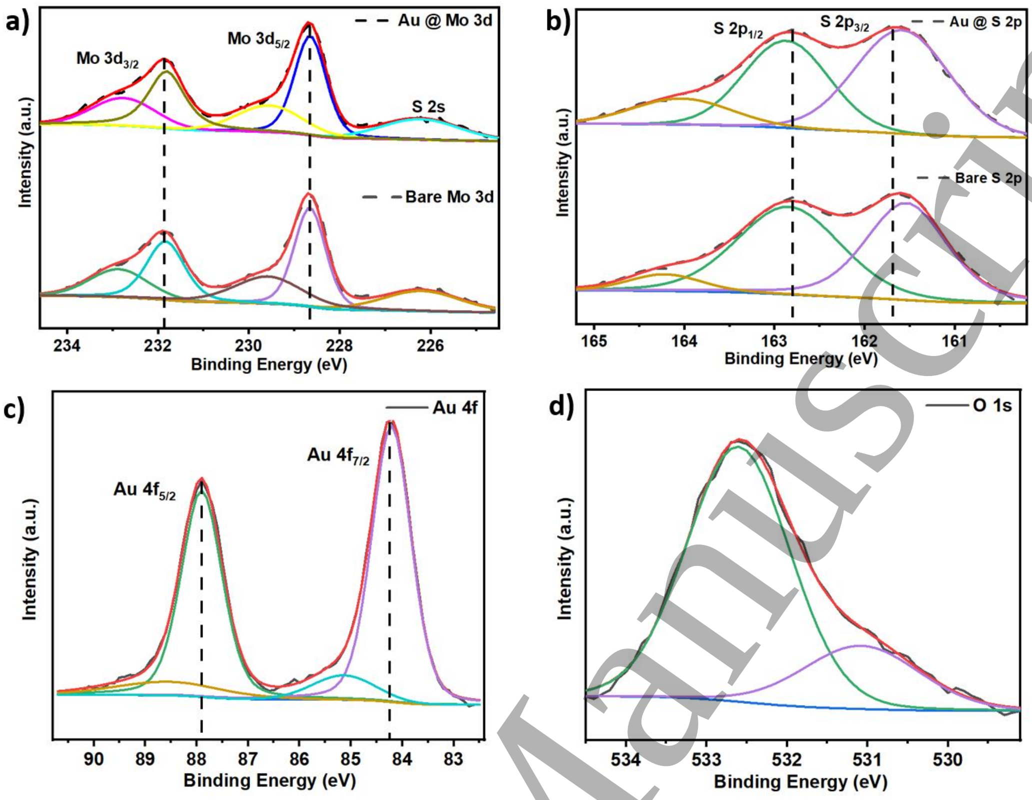

Figure4: X-ray photoelectron spectroscopy of bare MoS_2 and Au-MoS_2 hybrids: (a)Mo 3d (b)Au 4f (c)S 2p (d)O 1s. The peaks confirmed the presence of Mo, S and Au. The Schottky barrier formation and electrical interaction at the Au-MoS_2 hybrid interface are shown by a lower shift in binding energy.

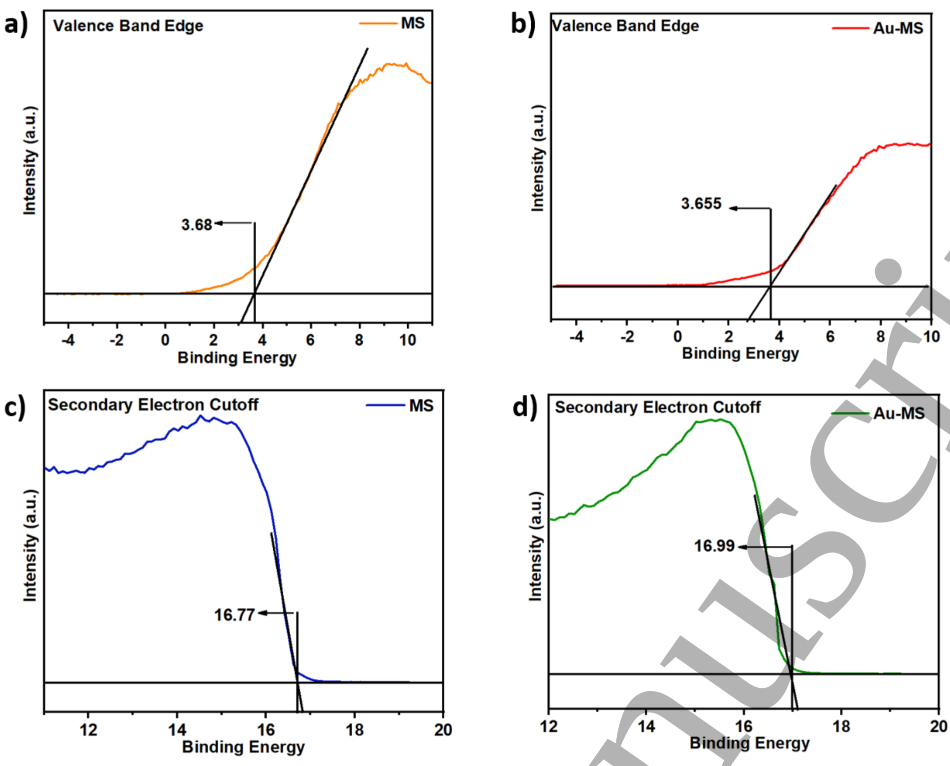

Figure5: UPS spectra of MoS_2 hybrids. By projecting the low binding energy edge to the baseline, the intercept on the abscissa was used to estimate the valence band maximum for each spectrum.

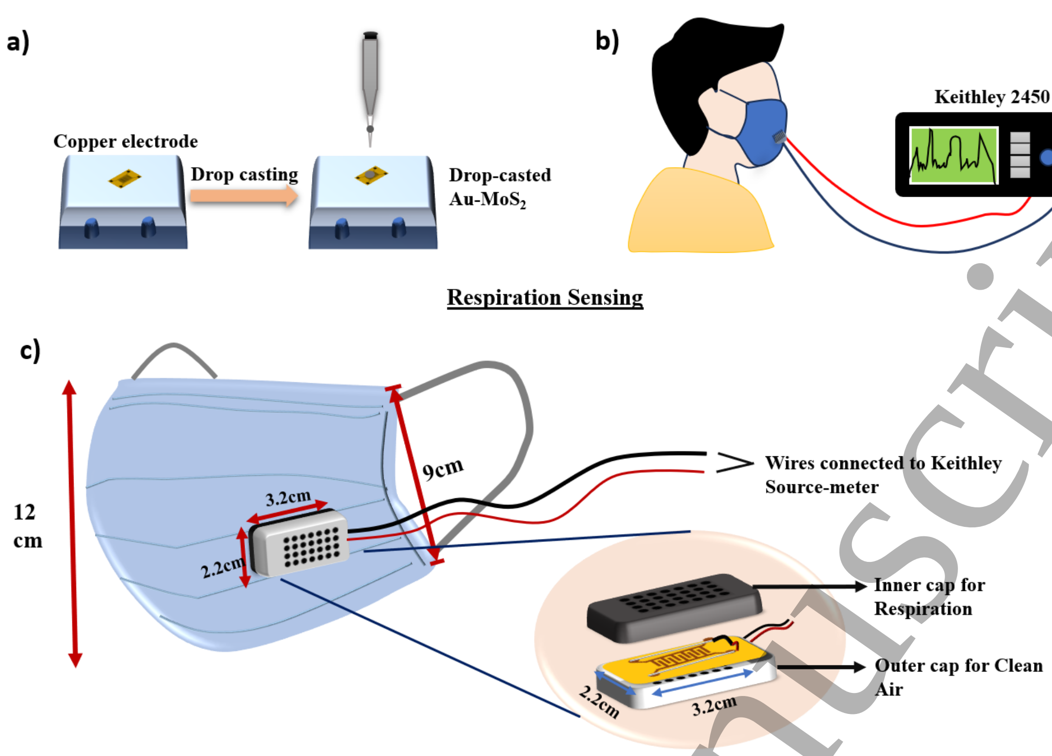

Figure 6: Schematic representation of: (a) Drop-casting on PCB Copper electrodes (b) monitoring human respiration by Keithley source-meter (c) Respiratory sensor integrated into a mask.

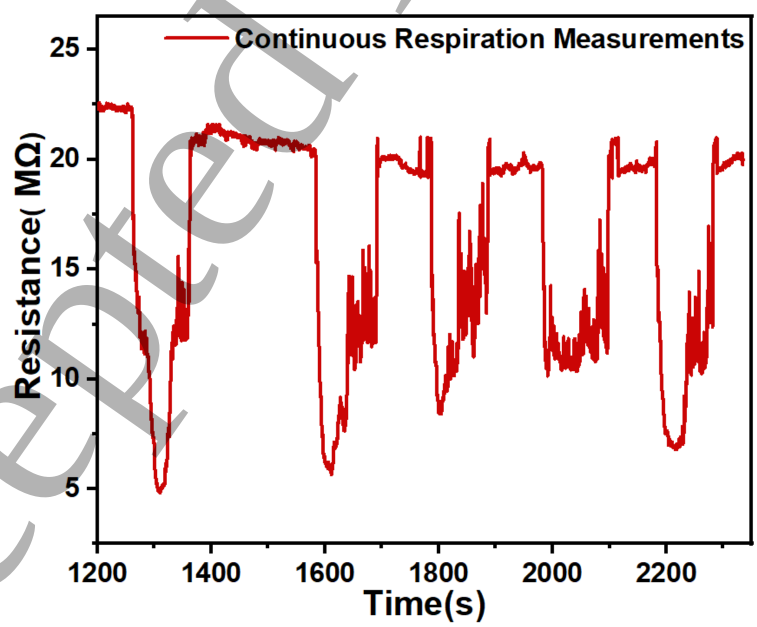

Figure 7: Repeatability performance of the sample.

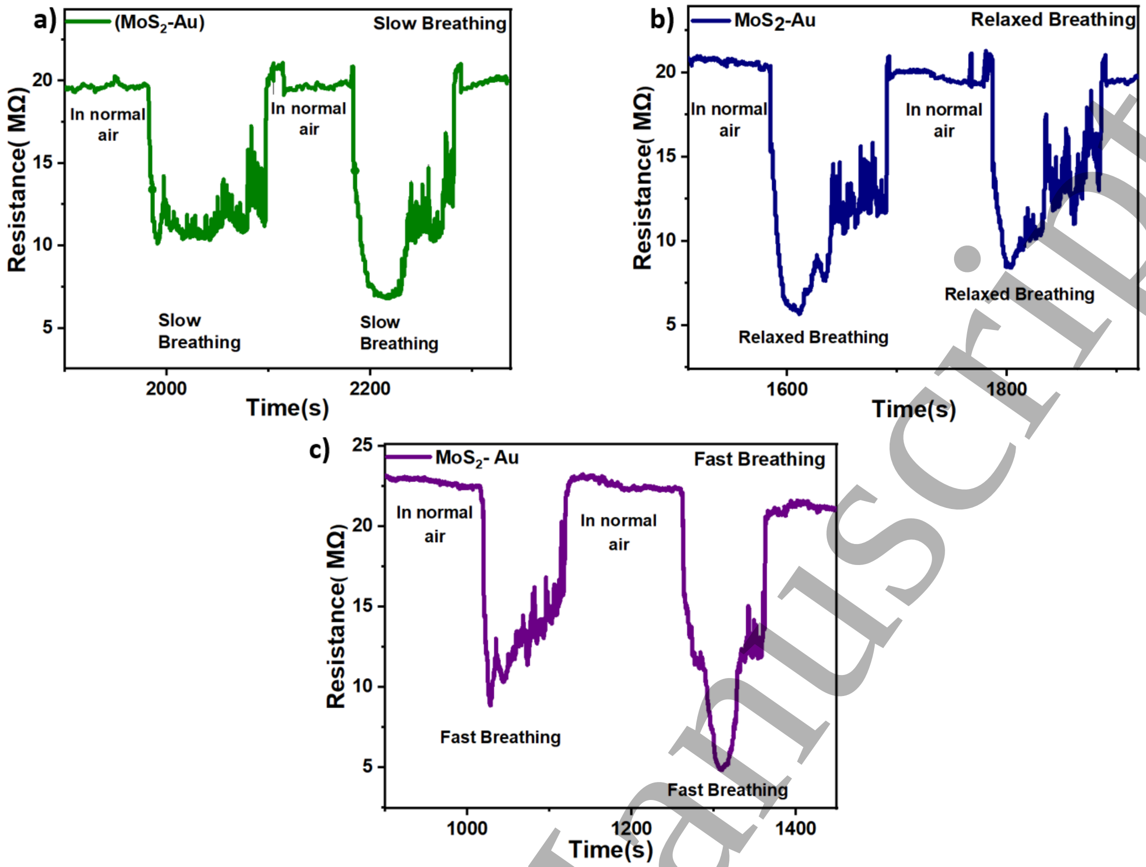

Figure8: Response curve of the respiratory sensor (a)Slow breathing (b)Relaxed breathing (c)Fast breathing.

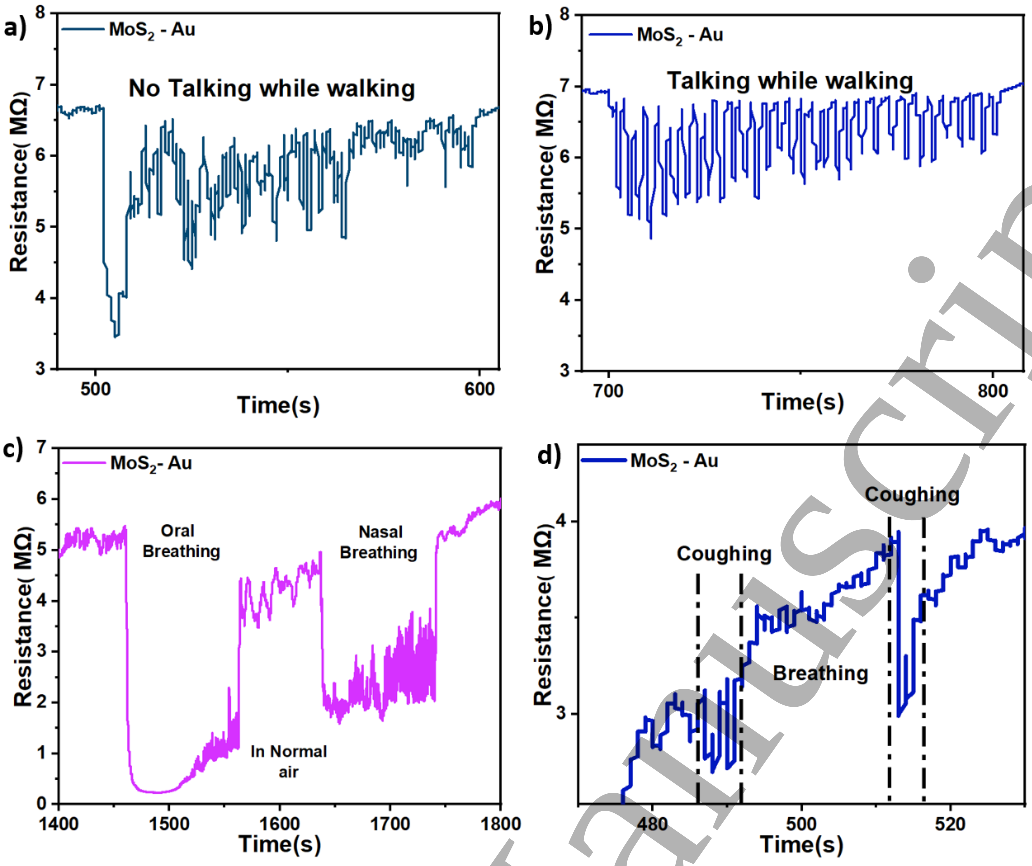

Figure9: Response curve at different parameters: (a) No talking while walking (b) Talking while walking (c) Coughing (d) Oral-Nasal Breathing. These parameters showed a variety of patterns as observed by Au-MoS_2 based respiratory sensors.

Serial Number	Element	Sensor Type	Location	Measured Parameter	Reference
1)	Silver Coated Nylon Thread	Antenna Based Sensor	Chest	Resonance Frequency Shift	[37]
2)	Conductive Polymer	Antenna Based Sensor	Wearable Sensor	Impedance and Resonance Frequency	[38]
3)	Au-MoS_2 hybrid gas sensor	Resistive Type Sensor	-	Resistance	[19]
4)	Silver Coated Embroided Textile	Capacitance Based Sensor	Abdomen	Capacitance	[39]
5)	Textile based capacitor with interdigitated electrodes (IDE)	Capacitance Based Sensor	Nose and Mouth	Capacitance	[40]
6)	Silver Thread Capacitor	Capacitance Based Sensor	Abdomen	Capacitance	[41]

Figure10: Table showing the variation of sensors on previous work.

References

[1] Al-Khalidi F Q, Saatchi R, Burke D, Elphick H and Tan S 2011 Respiration rate monitoring methods: A review *Pediatr Pulmonol* **46** 523–9

[2] Kim H S, Kang J H, Hwang J Y and Shin U S 2022 Wearable CNTs-based humidity sensors with high sensitivity and flexibility for real-time multiple respiratory monitoring *Nano Converg* **9**

[3] Chu M, Nguyen T, Pandey V, Zhou Y, Pham H N, Bar-Yoseph R, Radom-Aizik S, Jain R, Cooper D M and Khine M 2019 Respiration rate and volume measurements using wearable strain sensors *NPJ Digit Med* **2**

[4] Li D, Lu H, Qiu W, Dong J, Guan H, Zhu W, Yu J, Luo Y, Zhang J and Chen Z 2017 Molybdenum disulfide nanosheets deposited on polished optical fiber for humidity sensing and human breath monitoring *Opt Express* **25** 28407

[5] Burman D, Sharma A and Guha P K 2018 Flexible Large MoS2 Film Based Ammonia Sensor *IEEE Sens Lett* **2**

[6] Li Y, Zhang M, Hu X, Yu L, Fan X, Huang C and Li Y 2021 Graphdiyne-based flexible respiration sensors for monitoring human health *Nano Today* **39**

[7] Rittersma Z M *Recent achievements in miniaturised humidity sensorsÐa review of transduction techniques*

[8] Zhang D, Wang M, Zhang W and Li Q 2020 Flexible humidity sensing and portable applications based on MoSe2 nanoflowers/copper tungstate nanoparticles *Sens Actuators B Chem* **304**

[9] Solanki S, Soni A, Pandey M K, Biradar A and Sumana G 2018 Langmuir-Blodgett Nanoassemblies of the MoS2-Au Composite at the Air-Water Interface for Dengue Detection *ACS Appl Mater Interfaces* **10** 3020–8

[10] Senthil P, Sankar A, Sakthilatha D and Saravanan S P 2023 Fabricated Au NPs/MoS2@rGO multidimensional hybrid photocatalyst for enhanced H2 evaluation reaction performance under UV light *Journal of Materials Science: Materials in Electronics* **34**

[11] Shi Y, Huang J K, Jin L, Hsu Y Te, Yu S F, Li L J and Yang H Y 2013 Selective decoration of Au nanoparticles on monolayer MoS 2 single crystals *Sci Rep* **3**

[12] Wang J, Zhou Q, Lu Z, Wei Z and Zeng W 2019 Gas sensing performances and mechanism at atomic level of Au-MoS2 microspheres *Appl Surf Sci* **490** 124–36

[13] Mondal S, Kim S J and Choi C G 2020 Honeycomb-like MoS2 Nanotube Array-Based Wearable Sensors for Noninvasive Detection of Human Skin Moisture *ACS Appl Mater Interfaces* **12** 17029–38

[14] Adeel M, Cotur Y, Naik A, Gonzalez-Macia L and Güder F 2022 Face masks as a platform for wearable sensors *Nat Electron* **5** 719–20

[15] Chen P, Hu J, Yin M, Bai W, Chen X and Zhang Y 2021 MoS2Nanoflowers Decorated with Au Nanoparticles for Visible-Light-Enhanced Gas Sensing *ACS Appl Nano Mater* **4** 5981–91

[16] Chen Z and Lu C 2005 Humidity sensors: A review of materials and mechanisms *Sens Lett* **3** 274–95

[17] Farahani H, Wagiran R and Hamidon M N 2014 Humidity sensors principle, mechanism, and fabrication technologies: A comprehensive review *Sensors (Switzerland)* **14** 7881–939

[18] Rawat S, Bamola P, Rani C, Kaushik V, Kumar U, Dwivedi C, Rattan R, Sharma M, Kumar R and Sharma H 2023 Interdigitated electrodes-based Au-MoS2 hybrid gas sensor for sensing toxic CO and NH3 gases at room temperature *Nanotechnology* **34**

[19] Yu X, Shiraki T, Yang S, Ding B and Nakashima N 2015 Synthesis of porous gold nanoparticle/MoS2 nanocomposites based on redox reactions *RSC Adv* **5** 86558–63

[20] Rawat S, Bamola P, Negi S, Karishma N, Rani C, Dangwal S, Mishra A, Khanuja M, Yogi A K, Chhoker S, Sharma M, Dwivedi C, Kumar R and Sharma H 2024 Light-Assisted AgMoS2 and PdMoS2 Hybrid Gas Sensors for Room-Temperature Detection of Ammonia *ACS Appl Nano Mater* **7** 746–55

[21] Rana D S, Kalia S, Thakur N, Singh R K, Kumar R and Singh D 2023 Synthesis of reduced graphene oxide-molybdenum disulfide nanocomposite as potential scaffold for fabrication of efficient hydrazine sensor *Mater Chem Phys* **294**

[22] Savjani N, Lewis E A, Bissett M A, Brent J R, Dryfe R A W, Haigh S J and O'Brien P 2016 Synthesis of Lateral Size-Controlled Monolayer 1H-MoS2@Oleylamine as Supercapacitor Electrodes. *Chemistry of Materials* **28** 657–64

[23] Singha S S, Mondal S, Bhattacharya T S, Das L, Sen K, Satpati B, Das K and Singha A 2018 Au nanoparticles functionalized 3D-MoS2 nanoflower: An efficient SERS matrix for biomolecule sensing *Biosens Bioelectron* **119** 10–7

[24] Pereira N M, Rezende N P, Cunha T H R, Barboza A P M, Silva G G, Lippross D, Neves B R A, Chacham H, Ferlauto A S and Lacerda R G 2022 Aerosol-Printed MoS2Ink as a High Sensitivity Humidity Sensor *ACS Omega* **7** 9388–96

[25] Ren J, Guo B, Feng Y and Yu K 2020 Few-layer MoS2 dendrites as a highly active humidity sensor *Physica E Low Dimens Syst Nanostruct* **116**

[26] Hou C, Tai G, Liu Y, Wu Z, Wu Z and Liang X 2021 *Electronic Supplementary Material (ESI) for Supplementary Material Ultrasensitive Humidity Sensing and their Multifunctional Applications of Borophene-MoS 2 Heterostructures*

[27] Kim Y, Kang S K, Oh N C, Lee H D, Lee S M, Park J and Kim H 2019 Improved Sensitivity in Schottky Contacted Two-Dimensional MoS2 Gas Sensor *ACS Appl Mater Interfaces* **11** 38902–9

[28] Wang B, Yang D, Chang Z, Zhang R, Dai J and Fang Y 2022 Wearable bioelectronic masks for wireless detection of respiratory infectious diseases by gaseous media *Matter* **5** 4347–62

[29] Dinh T, Nguyen T, Phan H P, Nguyen N T, Dao D V and Bell J 2020 Stretchable respiration sensors: Advanced designs and multifunctional platforms for wearable physiological monitoring *Biosens Bioelectron* **166**

[30] Kundu S K, Kumagai S and Sasaki M 2013 A wearable capacitive sensor for monitoring human respiratory rate *Japanese Journal of Applied Physics* vol 52

[31] Wang S, Jiang Y, Tai H, Liu B, Duan Z, Yuan Z, Pan H, Xie G, Du X and Su Y 2019 An integrated flexible self-powered wearable respiration sensor *Nano Energy* **63**

[32] Li W, Xu H, Zhai T, Yu H, Chen Z, Qiu Z, Song X, Wang J and Cao B 2017 Enhanced triethylamine sensing properties by designing Au@SnO2/MoS2 nanostructure directly on alumina tubes *Sens Actuators B Chem* **253** 97–107

[33] Thakur U N, Bhardwaj R and Hazra A 2021 Statistical Analysis for Selective Identifications of VOCs by Using Surface Functionalized MoS2 Based Sensor Array (MDPI AG) p 35

[34] Pang Y, Jian J, Tu T, Yang Z, Ling J, Li Y, Wang X, Qiao Y, Tian H, Yang Y and Ren T L 2018 Wearable humidity sensor based on porous graphene network for respiration monitoring *Biosens Bioelectron* **116** 123–9

[35] Shakya J, Patel A S, Singh F and Mohanty T 2016 Composition dependent Fermi level shifting of Au decorated MoS2 nanosheets *Appl Phys Lett* **108**

[36] Yan H, Song P, Zhang S, Zhang J, Yang Z and Wang Q 2016 A low temperature gas sensor based on Au-loaded MoS2 hierarchical nanostructures for detecting ammonia *Ceram Int* **42** 9327–31

[37] El Gharbi M, Fernández-García R and Gil I 2022 Embroidered wearable Antenna-based sensor for Real-Time breath monitoring *Measurement (Lond)* **195**

[38] Ahadi M, Roudjane M, Dugas M A, Miled A and Messaddeq Y 2022 Wearable Sensor Based on Flexible Sinusoidal Antenna for Strain Sensing Applications *Sensors* **22**

[39] Kim J and Kim J 2023 Classification of Breathing Signals According to Human Motions by Combining 1D Convolutional Neural Network and Embroidered Textile Sensor *Sensors* **23**

[40] Simić M, Stavrakis A K, Sinha A, Premčevski V, Markoski B and Stojanović G M 2022 Portable Respiration Monitoring System with an Embroidered Capacitive Facemask Sensor *Biosensors (Basel)* **12**

[41] Kim J S, Truong T T N and Kim J 2023 Development of Embroidery-Type Sensor Capable of Detecting Respiration Using the Capacitive Method *Polymers (Basel)* **15**